INITIATION AND PROPAGATION OF ERUPTIVE SOLAR FLUX LOOPS: INTERPLANETARY CONSEQUENCES

J. Chen and D. A. Garren

Beam Physics Branch, Code 6790, Plasma Physics Division
Naval Research Laboratory, Washington, DC 20375

Abstract. We have developed a theoretical model to study the origin and propagation of interplanetary magnetic clouds. The magnetic topology of the initial structure is that of an equilibrium flux loop with twisted field lines, a simple but fully three-dimensional (3D) configuration. The motion of the loop is triggered by emergence or injection of poloidal magnetic flux associated with the toroidal (loop-aligned) current. The resulting structures in the heliosphere closely resemble observed magnetic clouds. The main forces responsible for the dynamics are the Lorentz force ($\mathbf{J} \times \mathbf{B}$) and pressure force ($\nabla p$) acting on curved current-carrying plasma volumes.

1. Introduction

It is well known that coronal mass ejections (CMEs) play a major role in initiating geomagnetic activity and are associated with large nonrecurrent geomagnetic storms [e.g., *Joselyn and McIntosh*, 1981; *Wright and McNamara*, 1983; *Tsurutani et al.*, 1988; *Gosling et al.*, 1991; *Gosling*, 1993]. A significant subclass of CMEs are magnetic clouds, which have been identified by smooth rotation of magnetic field through large angles, lower temperatures, and a significant enhancement of magnetic field strength [*Burlaga et al.*, 1981]. The characteristic smooth rotation of magnetic field has led to the inference that clouds are magnetic flux loops with twisted field lines [*Klein and Burlaga*, 1982] and possibly connected to the Sun [*Burlaga et al.*, 1990]. Magnetic clouds constitute perhaps 1/3 of all CMEs [*Gosling*, 1990]. Because of the smooth rotation of the magnetic field, magnetic clouds can impose long periods of southward interplanetary magnetic field (IMF) on the magnetosphere, leading to efficient coupling between solar wind and the magnetosphere. As a result, they are closely associated with major geomagnetic storms [*Burlaga et al.*, 1987; *Tsurutani et al.*, 1988].

The local field properties in clouds have been modeled using cylindrically symmetric pinch equilibria [*Burlaga*, 1988; *Suess*, 1988], and *Farrugia et al.* [1993] studied the expansion of clouds previously reported by *Klein and Burlaga* [1982]. These models focused on the local equilibrium properties of clouds where they are observed in the heliosphere. The actual properties, however, depend on the initial solar structures and the propagation through and interaction with the ambient medium. Thus, it is necessary to understand the forces responsible for this dynamical process. Recently, *Chen and Garren* [1993] developed a dynamical model of magnetic clouds in which a toroidal flux loop is driven from its initial equilibrium in the corona, through the interplanetary medium, to 1 AU and beyond. The essence of this model is the $\mathbf{J} \times \mathbf{B}$ and ∇p forces acting on curved ("toroidal") magnetic flux loops with twisted field lines, and the major radial and minor radial expansions are calculated. The macroscopic properties of the resulting structures closely resemble those of the observed magnetic clouds.

2. The Model

The initial structure is taken to be a magnetic flux loop, which is approximated as a section of a circular torus. The essential physics of this model is the toroidal "hoop" force. The force acting on a section of the loop is nonlocal and depends on the current distribution of the entire loop [*Garren and Chen*, 1994]. The basic force has been discussed previously [*Chen*, 1989], and this article is based on the application of this force to the dynamics of magnetic clouds discussed in *Chen and Garren* [1993], hereafter Paper 1. The structure and force calculation are simplified but fully three-dimensional.

The magnetohydrodynamic (MHD) force density is

$$\mathbf{f} = (1/c)\mathbf{J} \times \mathbf{B} - \nabla p + \rho \nabla \phi, \tag{1}$$

where $\nabla \times \mathbf{B} = (4\pi/c)\mathbf{J}$. Here, ρ is the mass density, and ϕ is the gravitational potential. The loop above the photosphere may be thought of as a section of a torus characterized by major radius R and minor radius a. Integrating the force density $\mathbf{f}$ over a toroidal segment, we obtain the net force per unit length along the major radius

$$F_R = \frac{I_t^2}{c^2 R}\left[\ln\left(\frac{8R}{a}\right) + \frac{1}{2}\beta_p - \frac{1}{2}\frac{\overline{B_t}^2}{B_p^2} + 2\left(\frac{R}{a}\right)\frac{B_s}{B_p} - 1 + \frac{\xi_i}{2}\right] - F_g - F_d, \tag{2}$$

where $\beta_p = 8\pi(\overline{p} - p_a)/B_p^2$, $\overline{p}$ is the average pressure inside the loop, p_a is the ambient coronal pressure, $\overline{B_t}$ the average toroidal field inside the loop, $B_p = B_p(a)$, and ξ_i is the internal inductance characterizing the toroidal current distribution inside the loop. The ambient field has a component B_s normal to the plane of the loop. Quantities inside (outside) the loop are denoted by bars (subscript a). The drag term in (2) has the form

$$F_d = c_d[n_a m_i a(V - V_a)|V - V_a|]. \tag{3}$$

where V is the major radial velocity, V_a is the local flow speed of the ambient solar wind, and c_d is the drag coefficient which in general is a function of velocity. The term

Proc. of the Third SOHO Workshop – Solar Dynamic Phenomena and Solar Wind Consequences, held at Estes Park, Colorado, USA, 26 – 29 September 1994 (ESA SP-373, December 1994)

F_g is the gravitational force per unit length. At the apex, we have

$$F_g = \pi a^2 mg(Z)(\overline{n} - n_a), \tag{4}$$

where it is along the major radius. The gravitational acceleration at the apex is given by

$$g(Z) = g_0/(1 + Z/R_\odot)^2, \tag{5}$$

where $g_0 = 2.74 \times 10^4$ cm/s^2 is the surface gravitational acceleration, $R_\odot \simeq 7 \times 10^5$ is the solar radius, and Z is the apex height above the photosphere.

In applying equation (2) to solar loops, we make a geometrical simplification that the loop above the photosphere is a section of a torus with uniform major radius R and fixed footpoint separation $2s_0$. In general, the toroidal foces in (2) depend on the global shape of the loop, but it can be shown that (2) is a good approximation for slender loops ($R \gg a$) which vary smoothly in the toroidal direction [*Garren and Chen*, 1994]. The assumption of uniform R can be written as

$$R = (Z^2 + {s_0}^2)/2Z, \tag{6}$$

where $2s_0 \ll R_\odot$. This simplification leads to the result that $R = 0.5$ AU when the apex reaches 1 AU (Paper 1). Comparing this result with observationally inferred major radus of 0.3 AU [*Burlaga et al.*, 1990], we see that the large-scale shape of the model loop is consistent with observed structures. We also expect that as a loop becomes large, the exact shape near the footpoints will have less influence on the dynamics of the apex.

The apex motion is governed by

$$M\frac{d^2Z}{dt^2} = F_R, \tag{7}$$

where $M = \pi a^2 \overline{n} m_i$ and the major radial velocity of center of mass of the apex is given by $V \equiv dZ/dt$. The expansion of the rest of the loop is determined from (6), subject to the constraint that s_0 remains fixed in time. The footpoints are assumed to be immobile because of the massive photospheric density ($\sim 10^{16-17}$ cm^{-3}) relative to that of the corona ($\sim 10^8$–10^{10} cm^{-3}). However, we specifically do not assume infinite photospheric conductivity, and the subphotospheric portion of the structure can serve as a flux or energy reservoir [*Chen*, 1989]. We require no particular current distribution below the photosphere but only that current be conserved. The minor radius of the apex $a(t)$ satisfies

$$M\frac{d^2a}{dt^2} = \frac{{I_t}^2}{c^2 a}\left(\frac{\overline{B_t}^2}{{B_p}^2} - 1 + \beta_p\right). \tag{8}$$

This equation is obtained by integrating (1) in the minor radial direction and describes a locally straight cylindrical pinch if $a \ll R$.

Given a current loop, we can define the poloidal flux above the photosphere by $\Phi = L_p I_t$, with the loop self-inductance approximated by

$$L_p = \frac{4\pi\Theta R}{c^2}\left[\ln\left(\frac{8R}{a}\right) - 2\right],$$

where $2\pi\Theta R$ is the arc length of the loop between the two footpoints. Here, $\Theta = 1 - \theta/\pi$ for $Z \geq s_0$ and $\Theta = \theta/\pi$ for $Z < s_0$, where 2θ is the angular separation of the footpoints. For the initial loop, we take a to be constant along the loop so that the magnetic energy $(1/2)L_p {I_t}^2$ is uniformly distributed along the loop above the photosphere. As the loop expands, this approximation becomes invalid because the apex minor radius a_a becomes significantly greater than that near the footpoints, a_f. Thus, we will use an effective loop inductance

$$L = (L_a + L_f)/2, \tag{9}$$

where L_a and L_f are the values of L_p using, respectively, a_a and a_f. This simplification includes the essential point that a varies by a few orders of magnitude along the loop. Because a_a is much greater than a_f, the magnetic energy becomes more concentrated near the footpoints. In contrast, the fractional R variation is substantially smaller, and the logarithmic dependence in L makes the R variation relatively unimportant. Physically, equation (9) implies that the apex cannot access the energy of the entire loop. For a more exact expression for the inductance of an arbitrary slender ($R/a \gg 1$) loop, see *Landau et al.* [1984].

In our model, we specify $d\Phi(t)/dt$. In this paper, we do not address the question of what physical processes determine $\Phi(t)$. A suggested scenario is redistribution of subphotospheric magnetic energy, resulting in surface manifestations such as eruption of loops and flares [*Chen*, 1989, 1990]. Possible subphotospheric dynamics and energy transport mechanisms will not be considered here. If the photosphere were infinitely conducting, $d\Phi/dt$ would be nearly zero on the time scale of interest. (The conventional paradigm is that the slow twisting of the footpoint field lines can quasi-statically increase Φ over days.)

Finally, we adopt the equation of state

$$\frac{d}{dt}\left(\frac{\overline{p}}{\overline{\rho}^\gamma}\right) = 0. \tag{10}$$

inside the loop. In Paper 1, $\gamma \simeq 1$ was used based on the assumption that the thermal conductivity parallel to magnetic field is high and that the loop remains connected to the Sun. Comparing this assumption with $\gamma = 5/3$, it was found that the overall propagation properties are not significantly influenced by the γ values but that the temperature of the loop decreased to a few degrees K at 1 AU if adiabatic expansion was assumed. This result is insensitive to the magnetic topology, and Paper 1 concluded that magnetic clouds and CMEs with the observed temperature of several times 10^4 K to 10^5 K must maintain magnetic and thermal connection with the Sun. As before, we will use $\gamma = 1.1$ in the present paper. Thus, the loop dynamics is described by the equations of motion, (7) and (8), constrained by $\Phi(t)$ and equation (10).

For the interplanetary medium, we adopt a simple model. The average solar wind speed is prescribed and is ramped up from zero to the asymptotic value V_{sw} using hyperbolic tangent profiles. We will discuss examples with $V_{sw} = 400$ km/s and $V_{sw} = 600$ km/s. For $Z < 7R_\odot$, we assume $p_a \propto \exp(-Z/H)$ where $H = 2kT_a/mg$ with the local temperature T_a and local gravitational acceleration g. Beyond $7R_\odot$, spherical divergence $(Z + R_\odot)^{-2}$ is also

imposed on p_a, and we take $T_a \propto (Z + R_\odot)^{-\alpha}$ [e.g., *Marsch*, 1990] with $\alpha = 0.3$. In Paper 1, V_a was ramped up to 400 km/s between $7R_\odot$ and $\sim 40R_\odot$. In comparison, the model loops have larger minor radii at 1 AU if the solar wind speed reaches 400 km/s at $10R_\odot$.

3. Results

Equations (7) and (8) describe the dynamics of the apex, as constrained by the momentum coupling with the ambient plasma, equation (3), the global geometry, equation (6), and the equation of state (10). In this model, the initial equilibrium is set in motion by increasing the toroidal (loop-aligned) current. This is equivalent to increasing the poloidal flux Φ and is a particular form of emerging flux in which the flux given by the current in the loop increases. This is to be distinguished from emergence of flux attributable to a separate current distribution. The latter form of emerging flux does not change Φ. It can be shown that the loop can only oscillate about its initial equilibrium if $d\Phi/dt = 0$ [*Chen*, 1989, 1990]. In response to an increasing Φ, the loop apex rises, and the minor radius expands. Figure 1 illustrates the form of $\Phi(t)$ and the resulting dynamics of a model loop for the initial 180 min. Note that the apex travels at ~200 km/sec for a few hours (Figure 2b). The velocity decreases from the initial peak of ~300 km/sec because the expanding major radius R causes J_t to decrease. The minor radius exhibits small amplitude oscillations as discussed previously [*Chen*, 1989; *Cargill et al.*, 1994a]. The subsequent evolution of this model loop has been discussed in Paper 1 and will not be reproduced here.

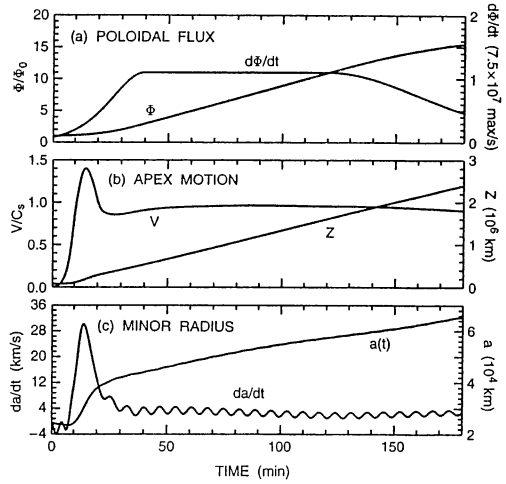

Figure 1. Early-time evolution. From *Chen and Garren* [1993]. (a) poloidal flux $\Phi(t)$ and flux injection rate $d\Phi/dt$. (b) Apex velocity and height. $C_s = 235$ km/sec. (c) Minor radial dynamics, $a(t)$.

The long-time dynamics of the loop depends on the ambient plasma through the momentum coupling given by the drag term, equation (3). Figure 2 shows two solar wind speed profiles: (A) the solar wind speed is ramped up to $V_{sw} = 400$ km/sec at $\sim 10R_\odot$ and (B) the solar wind reaches $V_{sw} = 600$ km/sec at $\sim 20R_\odot$. These profiles are motivated by those given by other researchers [e.g., *Coles et al.*, 1991]. Figure 3 describes the long-time dynamics of one model loop for the two solar wind velocity profiles.

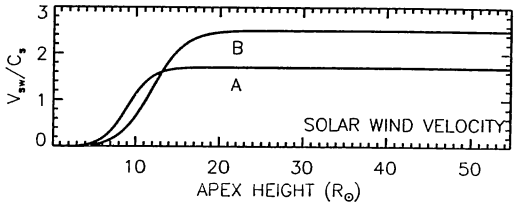

Figure 2. Solar wind speed profiles. The solar wind speed is ramped up to V_{sw} using a hyperbolic tangent form. (A) $V_{sw} = 400$ km/sec. (B) $V_{sw} = 600$ km/sec.

The labels A and B correspond to the profiles A and B in Figure 2. The basic dynamics are similar to those described in Paper 1. The major difference is that the solar wind speed was ramped up to 400 km/sec at about $40–50R_\odot$. In the present examples, the loops reach 1 AU sooner, and the minor radius is approximately twice as large as that found previously. For both loops A and B, the loop size is $2a \gtrsim 0.2$ AU. The initial loop has a magnetic field strength of ~30 G, and at 1 AU, $B \simeq 15$ nT. The average propagation speed, transverse size, and the field strength are consistent with observations at 1 AU [*Lepping et al.*, 1990] for both solar wind profiles.

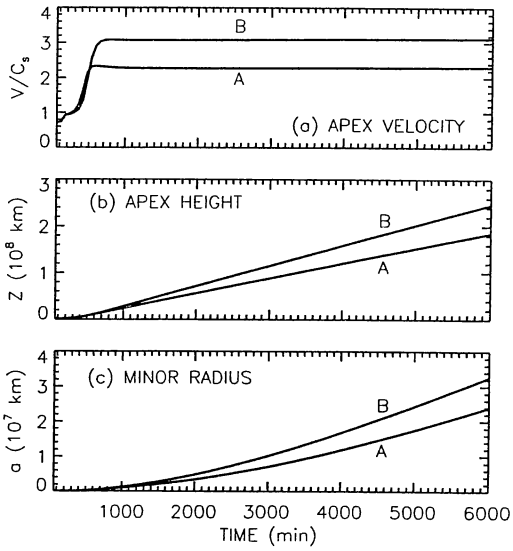

Figure 3. Long-time dynamics. A and B correspond to solar wind profiles A and B shown in Figure 2.

In both examples, the average speed of the loop is roughly 100 km/sec faster than the average ambient solar wind speed. In this model, this velocity differential ΔV occurs as the terminal velocity by balancing the driving force with the drag force in equation (2). Thus, ΔV depends on the loop geometry and B (or I_t). If the magnetic field strength is reduced, ΔV can be made small. Note that the velocity profiles of both model loops closely follow

the corresponding ambient solar wind velocity profiles after the initial acceleration periods. This is simply because of the momentum coupling arising from the drag term. It has been noted by *Gosling et al.* [1994] that the speeds of CMEs detected near 4 AU tend to be similar to the ambient solar wind speed profiles. During the initial eruptions, the speeds of CMEs can be considerably faster than the ambient plasma. The present results are consistent with these observed properties.

In addition to the macroscopic dynamical observables, we have examined the local magnetic field inside the loop but with the requirement that the integrated quantities match those obtained from the global dynamic model described above. We solve $(1/c)\,\mathbf{J} \times \mathbf{B} - \nabla p = 0$ for a straight cylinder subject to the constraints that the spatial scales are of the order of the minor radius a and that the current distribution vanish smoothly at $r = a$. Here, ∇p is not necessarily zero. A solution is given by

$$B_p(r) = 3B_p \left(\frac{r}{a}\right)\left(1 - \frac{r^2}{a^2} + \frac{r^4}{3a^4}\right), \qquad r \le a$$
$$= B_p \frac{a}{r}, \qquad r > a,$$

$$B_t(r) = 3B_t \left(1 - 2\frac{r^2}{a^2} + \frac{r^4}{a^4}\right), \qquad r \le a$$
$$= 0, \qquad r > a$$

where $B_p = B_p(a)$ and B_t is the average of $B_t(r)$ across the minor radius, with the relation $B_t(0) = 3B_t$. The toroidal loop model yields B_p, B_t, and a, which are used to specify the solution. The above field is due only to the current inside the loop and is qualitatively similar to the constant-α Lundquist solution previously obtained by *Burlaga* [1988]. To the extent that the force-free solution has no short scale lengths, it is a special case of our solutions. Note that this conclusion does not include interaction with the ambient plasma which can cause shocks and compression / deformation of flux loops, which will be treated separately [*Cargill et al.*, 1994b].

4. Discussion

We have developed a dynamic model of interplanetary magnetic clouds. The initial calculations presented here and previously [*Chen and Garren*, 1993] show that it is indeed possible for solar flux loops to evolve from the lower coronal environment to 1 AU and that the resulting structures closely resemble the observed magnetic clouds. If we adopt the view that solar prominences and filaments have the underlying magnetic topology of flux loops, the model results provide a theoretical basis for the empirical associations between eruptive filaments and magnetic clouds [*Wilson and Hildner*, 1984; *Rust*, 1994]. The forces responsible for the eruption and subsequent propagation is the Lorentz force $\mathbf{J} \times \mathbf{B}$ and pressure force ∇p. The initial equilibrium loop is set into motion by emergence of the poloidal flux associated with the increasing toroidal current. Inside the model loops, we have found non-force-free solutions which closely resemble those of observed clouds.

In these calculations, the minor cross-section is taken to be circular. Recently, we have carried out the first simulations of driving deformable magnetic flux loops through magnetized ambient plasmas that are consistent with the interplanetary medium [*Cargill et al.*, 1994b]. The objective is to understand the range of possible magnetic loop configurations as may be observable in the heliosphere. This is important because magnetic configuration is a key identifier of magnetic clouds and more generally CMEs.

Although the initial results are promising, there remain a number of important issues that are under investigation. One is the detailed dynamical properties within $30R_\odot$ which is the field of view of the LASCO instrument on SOHO. This is a particularly important property for investigating the forces responsible for the eruption of prominences and eruptions: $30R_\odot$ is a much larger field of view than that of any other data set, potentially providing an unsurpassed view of long-time dynamics of flux loops and CMEs. Such constraints constitute a more stringent observational challenge to theoretical models. The advantage of the present model is that it can give macroscopic observables such as the height and speed of the loop as functions of time to any heliocentric distances. Another area of investigation is the plasma dynamics preceding, during, and immediately following eruptions. A novel aspect of the model is that the eruption is triggered by emergence or injection of poloidal flux associated with the toroidal current. A recent simulation study suggests that plasmas at the photospheric density of $10^{16-17}\,\mathrm{cm}^{-3}$ should move only slowly (a few m/sec) but that at chromospheric densities of the order of $10^{11}\,\mathrm{cm}^{-3}$, emerging magnetic field can drive plasmas at much higher speeds, perhaps a few hundred km/sec [*Huba and Chen*, 1994]. Another issue of importance is the details of possible equilibrium structures. We are currently developing a fully three-dimensional MHD simulation model of magnetic flux loops [*Mobarry and Chen*, 1994]. The mechanism of flux injection and the response of the loop have yet to be fully explored.

Acknowledgments

This work was supported by the Office of Naval Research.

References

Burlaga, L. F., *J. Geophys. Res., 93*, 7217, 1988.

Burlaga, L. F., E. Sittler, F. Mariani, and R. Schwenn, *J. Geophys. Res., 86*, 6673, 1981.

Burlaga, L. F., K. W. Behannon, and L. W. Klein, *J. Geophys. Res., 92*, 5725, 1987.

Burlaga, L. F., R. R. Lepping, and J. A. Jones, in *Physics of Magnetic Flux Ropes*, *Geophys. Monogr. Ser.*, vol. 58, ed. by C.T. Russell, E.R. Priest, and L.C. Lee, p. 373, AGU, Washington, DC, 1990.

Cargill, P. J., J. Chen, and D. A. Garren, *Astrophys. J., 423*, 854, 1994a.

Cargill, P. J., J. Chen, D. S. Spicer, and S. T. Zalesak, *Geophys. Res. Lett.*, submitted, 1994b. Also this volume.

Chen, J., *Astrophys. J., 338*, 453, 1989.

Chen, J., in *Physics of Magnetic Flux Ropes*, *Geophys. Monogr. Ser.*, vol. 58, ed. by C. T. Russell, E. R. Priest, and L. C. Lee, p. 269, AGU, Washington, DC, 1990.

Chen, J. and D. A. Garren, *Geophys. Res. Lett., 20*, 2319, 1993.

Coles, W. A., R. Esser, U.-P. Lovhaug, and J. Markkanen, *J. Geophys. Res.*, *96*, 13849, 1991.
Farrugia, C. J., L. F. Burlaga, V. A. Osherovich, I. G. Richardson, M. P. Freeman, R. P. Lepping, and A. J. Lazarus, *J. Geophys. Res., 98*, 7621, 1993.
Garren, D. A. and J. Chen, *Phys. Plasmas*, *1*, 3425, 1994.
Gosling, J. T., in *Physics of Magnetic Flux Ropes*, *Geophys. Monogr. Ser.*, vol. 58, ed. by C.T. Russell, E.R. Priest, and L.C. Lee, p. 343, AGU, Washington, DC, 1990.
Gosling, J. T., *J. Geophys. Res.*, *98*, 18937, 1993.
Gosling, J. T., D. J. McComas, J. L. Phillips, and S. J. Bame, *J. Geophys. Res.*, *96*, 7831, 1991.
Gosling, J. T., S. J. Bame, D. J. McComas, J. L. Phillips, B. E. Goldstein, and M. Neugebauer, *Geophys. Res. Lett.*, *21*, 1109, 1994.
Huba, J. D. and J. Chen, *Astrophys. J.*, submitted, 1994.
Joselyn, J. A. and P. S. McIntosh, *J. Geophys. Res.*, *86*, 4555, 1981.
Klein, L. W. and L. F. Burlaga, *J. Geophys. Res., 87*, 613, 1982.
Landau, L. D., E. M. Lifshitz, and L. P. Pitaevskii, *Electrodynamics of Continuous Media*, 2nd edition, p. 124, Pergamon Press, Oxford, UK, 1984.
Lepping, R. P., J. A. Jones, and L. F. Burlaga, *J. Geophys. Res., 95*, 11,957, 1990.
Mobarry, C. M. and J. Chen, *EOS Suppl.* (abstract), 1994.
Marsch, E., in *Physics of the Inner Heliosphere* II, edited by R. Schwenn and E. Marsh, p. 45, Springer-Verlag, Berlin, 1991.
Rust, D. M., *Geophys. Res. Lett.*, *21*, 241, 1994.
Suess, S. T., *J. Geophys. Res., 93*, 5437, 1988.
Tsurutani, B. T., W. D. Gonzalez, F. Tang, S. I. Akasofu, and E. Smith, *J. Geophys. Res., 93*, 8519, 1988.
Wilson, R. M. and E. Hildner, *Solar Phys., 91*, 169, 1984.
Wright, C. S. and L. F. McNamara, *Solar Phys., 87*, 401, 1983.